AGU PUBLICATIONS

Geophysical Research Letters

RESEARCH LETTER
10.1002/2016GL067902

Key Points:
- Western North Pacific summer monsoon circulation
- Long-lead prediction skills of summer monsoon
- CMIP5 decadal hindcasts

Supporting Information:
- Supporting Information S1

Correspondence to:
S.-W. Son,
seokwooson@snu.ac.kr

Citation:
Choi, J., S.-W. Son, K.-H. Seo, J.-Y. Lee, and H.-S. Kang (2016), Potential for long-lead prediction of the western North Pacific monsoon circulation beyond seasonal time scales, *Geophys. Res. Lett.*, *43*, 1736–1743, doi:10.1002/2016GL067902.

Received 20 JAN 2016
Accepted 28 JAN 2016
Accepted article online 2 FEB 2016
Published online 19 FEB 2016

Potential for long-lead prediction of the western North Pacific monsoon circulation beyond seasonal time scales

Jung Choi[1], Seok-Woo Son[1], Kyong-Hwan Seo[2], June-Yi Lee[2], and Hyun-Suk Kang[3]

[1]School of Earth and Environmental Sciences, Seoul National University, Seoul, South Korea, [2]Department of Atmospheric Sciences, Pusan National University, Busan, South Korea, [3]National Institute of Meteorological Research, Jeju, South Korea

Abstract Although the western North Pacific (WNP) monsoon circulation significantly impacts the socioeconomic communities around Asia, its prediction is only limited to a few months. By examining the Coupled Model Intercomparison Project phase 5 decadal hindcast experiments, we explore a possibility of the extended prediction skill for the WNP monsoon circulation beyond seasonal time scales. It is found that the multimodel ensemble (MME) predictions, initialized in January, successfully predict the WNP circulation in spring and early summer. Somewhat surprisingly, a reliable prediction of the WNP circulation appears even in the following spring with a maximum lead time of 14 months. This unexpected prediction skill is likely caused by the improved El Niño–Southern Oscillation (ENSO) prediction and the exaggerated dynamical link between the ENSO and premonsoon circulation in the MME prediction. Although further studies are needed, this result may open up new opportunities for the multiseasonal prediction of the WNP monsoon circulation.

1. Introduction

The seasonal-to-interannual prediction of regional climate variability is known to have more important socioeconomic implications than the decadal or multidecadal climate projection, which has been extensively explored in the Intergovernmental Panel on Climate Change (IPCC) assessment report [*Intergovernmental Panel on Climate Change*, 2013]. For example, in South and East Asia, a reliable prediction of the western North Pacific (WNP) summer monsoon circulation several months in advance would be very beneficial [e.g., *Wang et al*., 2013]. This is especially true for water resource management, because the summer monsoon largely controls the annual precipitation in these regions. Recently, not only the summer season but also the spring-to-summer transition season has received an attention because the air-sea interaction and resulting anomalies over the WNP region from April to June play a crucial role in shaping the June–August WNP monsoon anomalies [e.g., *Hu et al*., 2014; *Wu and Hu*, 2015].

It is well documented that the prediction skill of summer monsoon precipitation is considerably low [e.g., *Lee et al*., 2010; *Seo et al*., 2015]. A reliable prediction is limited to only a month or two in the state-of-the-art seasonal prediction systems [*Lee et al*., 2011a, 2011b]. This limited prediction skill in precipitation is partly caused by the uncertainties of cloud physics and cumulus parameterizations in the models. In contrast, the large-scale atmospheric circulation associated with the WNP summer monsoon is known to be predictable with a longer lead time. For instance, the intensity of the western Pacific Subtropical High, which modulates the Asian summer monsoon system, can be qualitatively predicted with a maximum lead time of 5 months in fully coupled seasonal prediction systems [e.g., *Lee et al*., 2011b; *Li et al*., 2012; *Wang et al*., 2013].

This extended prediction skill of the monsoon circulation, which cannot be simply explained by atmospheric memory, is partly caused by the remote impacts from the tropical sea surface temperature (SST) variability. *Wang et al*. [2008] showed that the interannual variation of monsoon circulation over the WNP is strongly influenced by the El Niño–Southern Oscillation (ENSO), especially in the postsatellite era. In general, the WNP circulation in spring (March-April-May (MAM)) and in summer (June-July-August (JJA)) is negatively correlated with the previous winter's ENSO index. In other words, if the ENSO in the previous winter is in its warm phase, the WNP monsoon circulation in the following spring and summer seasons is often weaker than normal. This leads to a drier spring and summer over the WNP, but wetter seasons over East Asia.

In the state-of-the-art seasonal prediction models, ENSO prediction skill is typically about 6 months but can be extended to maximum 2 years in the select models [*Jin et al*., 2008; *Luo et al*., 2008; *Choi et al*., 2016]. By analyzing the Coupled Model Intercomparison Project phase 5 (CMIP5) decadal hindcast experiments [*Meehl et al*., 2014], *Choi et al*. [2016] recently showed that the multimodel ensemble (MME) prediction can predict ENSO up to 15 months in advance when the coupled model is initialized in January with the observed initial and boundary conditions. This extended prediction skill of ENSO suggests that the WNP circulation in spring and summer can be predicted beyond a seasonal time scale if the dynamic link between ENSO and monsoon circulations is well represented by the MME. This may potentiate the seamless seasonal-to-interannual prediction of the WNP monsoon circulation. This possibility is tested in the present study.

2. Data and Methodology

The summer monsoon circulation over the WNP has been quantified by several indices. Among many others, the Western North Pacific Monsoon (WNPM) index [*Wang et al*., 2001], which has been widely used in the literature, is utilized in this study to quantify the WNP circulation in both spring and summer. Briefly, this index measures the intensity of low-level circulations associated with the WNP subtropical high. In particular, it is defined by the horizontal shear of zonal wind at 850 hPa (U850) between the tropics averaged over 5°–15°N and 100°–130°E (southern box in Figure S1a in the supporting information) and the subtropics averaged over 20°–30°N and 110°–140°E (northern box in Figure S1a). The positive value (i.e., tropical minus subtropical U850 is positive) signifies cyclonic circulation near the South China Sea (see Figures S1c and S1d) and precipitation in the Southeast Asia (see Figures S1a and S1b).

The WNPM index prediction is evaluated for the CMIP5 decadal hindcast experiments. More than 10 models are available from the CMIP5 archive [*Meehl et al*., 2014]. Among them, only seven models (Table 1) that have been initialized every year since 1980 are used in this study as in *Choi et al*. [2016]. These models are BCC-CSM1-1 [*Wu et al*., 2014], CanCM4 [*Arora et al*., 2011], GFDL-CM2p1 [*Delworth et al*., 2006], MIROC5 [*Tatebe et al*., 2012], MPI-ESM-LR [*Matei et al*., 2012], and HadCM3 with anomaly initialization (HadCM3a) and full-field initialization (HadCM3f) [*Smith et al*., 2010]. Of these seven models, only the first five models, initialized in January, are used to calculate the MME predictions. The latter two models from HadCM3 were initialized in November and are examined separately to test the sensitivity to the initialization month. As summarized in Table 1, each model consists of at least three ensemble members. The five-model MME is computed using each model's ensemble mean value. Since the last initialization of BCC-CSM1-1 is January 2007, the MME prediction is evaluated from 1981 to 2007. In all analyses, a 3 month running mean is applied.

The model predictions are compared with the European Centre for Medium-Range Weather Forecasts Interim Reanalysis (ERA-Interim) [*Dee et al*., 2011] and the Global Precipitation Climatology Project (GPCP) [*Adler et al*., 2003] data sets. The ENSO prediction skill is evaluated by comparing the observed NINO3.4 SST with the model predictions. The observed NINO3.4 index is defined as the SST averaged over 5°S–5°N and 170°–120°W from the Extended Reconstructed Sea Surface Temperature Version 3b (ERSSTv3b) [*Smith et al*., 2008]. Both observational and decadal hindcast data are first interpolated to a uniform 2.5° × 2.5° grid to reduce uncertainty associated with different spatial resolution of each data. Bias adjustment is then applied to the model output in accordance to *International CLIVAR Project Office* [2011] to remove model drift [*Meehl et al*., 2014].

The prediction skills are evaluated by computing two deterministic metrics: the anomaly correlation coefficient (ACC) and mean squared skill score (MSSS), as proposed by *Goddard et al*. [2013]. The ACC is defined as

$$\mathrm{ACC}(\tau) = \frac{\frac{1}{n}\sum_{j=1}^{n}\left[H_{j\tau} - \overline{H}_{\tau}\right]\left[O_{j\tau} - \overline{O}_{\tau}\right]}{\sqrt{\frac{1}{n}\sum_{j=1}^{n}\left[H_{j\tau} - \overline{H}_{\tau}\right]^2}\sqrt{\frac{1}{n}\sum_{j=1}^{n}\left[O_{j\tau} - \overline{O}_{\tau}\right]^2}}. \quad (1)$$

Here observations (O) correspond to either gridded observations or reanalysis data. Each hindcast run can be represented by $H_{j\tau}$, in which H is the ensemble mean prediction, j is the initialization year ($j = 1 \sim n$, $n = 27$ for MME), and τ

Table 1. Description of the Models Used in This Study[a]

Name	Institution	Initialization		Number of Ensemble Members
		Type	Period (Number of Start Years, *n*)	
BCC-CSM1-1	BCC, China	Full field	Jan 1981–2007 (27)	3
CanCM4	CCCma, Canada	Full field	Jan 1981–2011 (32)	10
GFDL-CM2p1	NOAA GFDL, USA	Full field	Jan 1981–2011 (32)	10
MIROC5	AORI, Japan	Anomaly	Jan 1981–2010 (31)	6
MPI-ESM-LR	MPI-M, Germany	Anomaly	Jan 1981–2010 (31)	3
HadCM3a	Met Office, UK	Anomaly	Nov 1980–2009 (30)	10
HadCM3f	Met Office, UK	Full field	Nov 1980–2009 (30)	10

[a]An acronym follows those in the IPCC fifth assessment report.

is the forecast lead time. In equation (1), the climatological mean over 1981–2007 is denoted by an overbar. The MSSS, which is based on the mean squared error (MSE), is defined as

$$\mathrm{MSSS}(\tau) = 1 - \frac{\mathrm{MSE}_H(\tau)}{\mathrm{MSE}_{\overline{O}}(\tau)} = 1 - \frac{\frac{1}{n}\sum_{j=1}^{n}\left[\left(H_{j\tau} - \overline{H}_\tau\right) - \left(O_{j\tau} - \overline{O}_\tau\right)\right]^2}{\frac{1}{n}\sum_{j=1}^{n}\left(O_{j\tau} - \overline{O}_\tau\right)^2}. \quad (2)$$

Although both ACC and MSSS quantify the model bias, the MSSS is more focused on the magnitude of the bias. As shown in equation (2), it evaluates the model MSE against the observed MSE. For the perfect prediction, both ACC and MSSS are unity.

A reliable prediction skill is conventionally defined by ACC greater than 0.5–0.7 and MSSS greater than 0 (i.e., model MSE smaller than observed MSE). Following these criteria, we define the lower limit of prediction skill with ACC $\geq$ 0.5 and MSSS $\geq$ 0. Here both ACC and MSSS must be statistically significant at the 95% confidence level. Statistical significance is tested by a bootstrap method suggested by *Goddard et al*. [2013]. Both ensemble mean from each model's single integrations and skill scores (i.e., ACC and MSSS) are randomly calculated 1000 times at the same lead time. From the bootstrap-generated sample distributions of skill scores, the counted negative value ratio serves as the *p* value for the significance test. If the *p* value is lower than α, the skill score is considered to be significant at the $(1-\alpha)\times 100\%$ confidence level. We set α as 0.05, so if the counted negative values are less than 50 for 1000 samples, then the prediction skill score is statistically significant at the 95% confidence level. See *Goddard et al*. [2013] for the details.

3. Results

The observed time series of the WNPM index during the spring (MAM) and summer monsoon seasons (JJA) are depicted by black lines in Figures 1a and 1b, respectively. The springtime WNPM index is usually negative, because the monsoon region is located in the western boundary of the subtropical high (see Figure S1c). As the low-level westerly jet expands to the east in the summer, the WNPM index becomes positive (see Figure S1d). Here it is important to note that although the WNPM index quantifies the summer monsoon circulation over the western North Pacific, it also explains the low-level circulation and precipitation over the region in spring (Figures S1a and S1c). Moreover, it has been known that the WNP circulation in spring significantly controls the timing of the onset and mature structure of the Asian summer monsoon [*Joseph et al*., 1994; *Li and Yanai*, 1996].

Figures 1a and 1b also illustrate the predicted WNPM index in the spring and summer seasons for the first and second prediction years. Both spring and summer WNPM indices show strong interannual variations that are reasonably well predicted by the MME. The MME for the first prediction year explains 55% and 29% of the observed interannual variation in spring and summer WNPM indices, respectively. These values are statistically significant at the 95% confidence level, indicating that the WNP circulations in spring and summer are reasonably well predicted by the MME with a lead time of 2 months for the spring and 5 months for the summer. Somewhat surprisingly, a statistically significant relationship is also found even in the spring of the second prediction year. The R^2 in MAM of the second prediction year (14 lead months) is lower than that of the first prediction year, partly due to the reduction of the simulated ENSO amplitude in the second

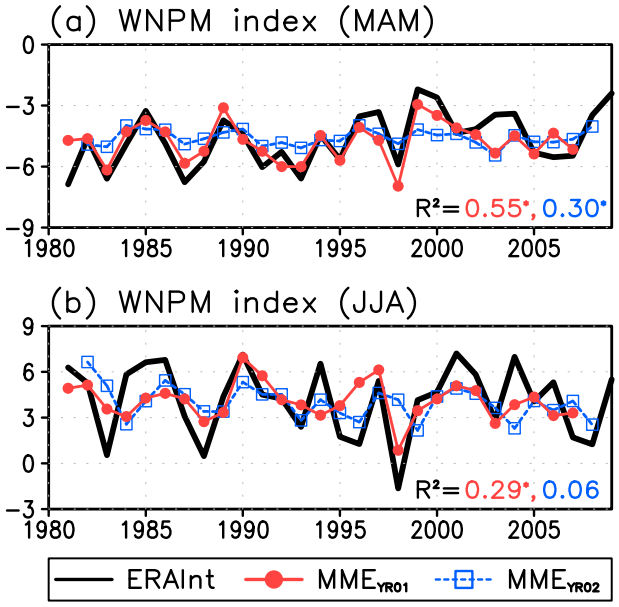

Figure 1. (a) Spring (MAM) WNPM index time series from ERA-Interim (black line) and CMIP5 MME of the first (red lines) and second (blue lines) prediction years. Units are m/s. (b) Same as Figure 1a but for the summer (JJA) season. R^2 is the percent of variance explained by the MME. An R^2 of 1 refers that the model perfectly reproduces the observed variance. R^2 that is statistically significant at the 95% confidence level is denoted by asterisks.

prediction year as discussed below [see also *Choi et al.*, 2016, Figure 8], but is still 0.30 that is comparable to that in JJA of the first prediction year (Figure 1).

To quantitatively evaluate MME prediction skill, ACC and MSSS are computed for the seasonal-to-interannual time scales in Figure 2a (2 lead months to 17 lead months), only spring and summer seasons are considered. Both metrics decrease with lead times and become statistically insignificant in the third prediction year. As anticipated from Figure 1a, the WNP circulation in spring is reliably predicted in the first prediction year (two lead months). ACC and MSSS are statistically significant and greater than 0.5 and 0.0, respectively.

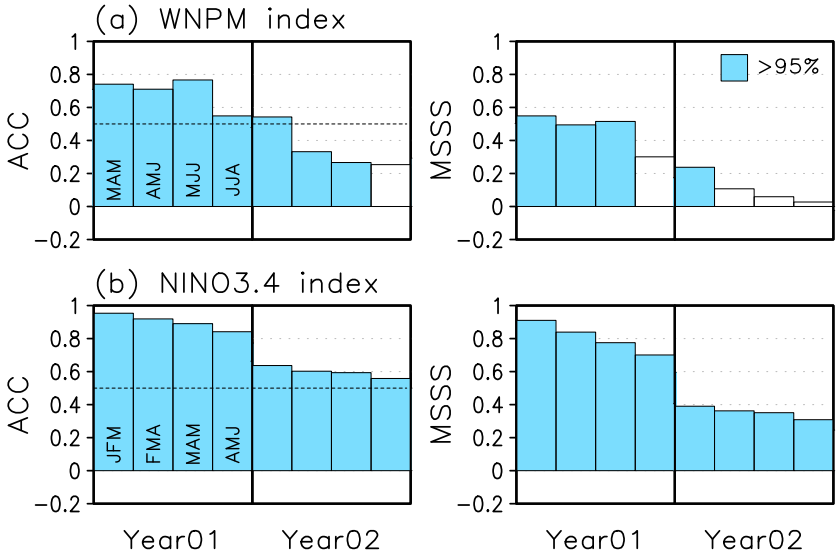

Figure 2. (a) The ACC and MSSS of the 3 month moving-averaged MME WNPM index. The prediction target covers from spring (MAM) to summer (JJA) seasons of the first and second years after the initialization in January. Shaded bars indicate values that are statistically significant at the 95% confidence level. (b) Same as Figure 2a but for NINO3.4 index from boreal late-winter (January-February-March (JFM)) to late-spring (April-May-June (AMJ)) seasons.

A significant ACC is also found in JJA (five lead months), while the MSSS is not statistically significant in this time lag. This indicates that the MME predicts the summer monsoon circulation in JJA only qualitatively. Therefore, it is concluded that WNP monsoon circulations are reliably predicted with a maximum lead time of 4 months (May-June-July (MJJ) in Figure 2a).

It is unclear what limits the prediction skill in summer monsoon circulation in the first prediction year. *Wang et al*. [2008] have shown a significant correlation between winter ENSO and WNP circulation in summer. One possible factor is a slow decaying of ENSO in the model. The predicted ENSO index has a longer *e*-folding time scale than observation (see Figure S2), exaggerating remote impact of equatorial SST on regional circulation over the WNP. Another factor might be the different air-sea interaction in spring and summer. Springtime circulation over the WNP is primarily controlled by the tropical Pacific SST [e.g., *Wang et al*., 2003], whereas summer monsoon circulation is influenced by the summer SST over the Indian Ocean [e.g., *Xie et al*., 2009] and the South China Sea (see Figure S3b). This seasonally varying air-sea coupling is not well reproduced by the MME predictions especially during the summer (Figures S3c and S3d).

In consistent with Figure 1a, a reliable prediction skill reappears in the second prediction year (Figure 2a). Both ACC and MSSS are statistically significant and greater than the threshold values in the second-year MAM. This result indicates that the WNP circulation in spring is predictable with a maximum lead time of 14 months when the January-initialized MME prediction is used. This result might be simply due to the long-term trend associated with global warming. To test the effect of long-term trend, the same analyses are repeated by filtering out the linear trend. The results are essentially the same (see Figure S4a), indicating that the extended prediction of the WNP circulation in MAM shown in Figure 2a is likely caused by the improved representation of the interannual variations of the WNP circulations in the MME predictions.

The above results suggest that springtime WNP circulations can be predicted a year in advance. If this is true, what is the possible source(s) of the improved and extended prediction skill? As discussed earlier, one possibility is the influence of the tropical SST. ENSO plays an important role on the interannual variability of the WNP monsoon circulations [e.g., *Wang et al*., 2008]. This implies that the statistically significant prediction skills of the spring WNP circulation in the second prediction year may be caused by the extended ENSO prediction skills. Figure 2b presents the ENSO prediction skills from late winter (January-February-March (JFM)) to late spring (April-May-June (AMJ)). Although not shown, the ENSO prediction skills rapidly decrease in the boreal spring (also known as spring predictability barrier) and increase again in the following winter [see *Choi et al*., 2016, Figure 10]. It is clear from Figure 2b that ENSO is well predicted by MME up to AMJ in the second prediction year (15 lead months). This ENSO prediction skill is comparable to or even better than the one reported in the literature [*Luo et al*., 2008; *Stockdale et al*., 2011]. Such an improved prediction skill is partly due to the MME approach instead of using a single model. As discussed below, the ENSO prediction skill of each model is generally worse than that of MME.

The dynamic link between the ENSO and springtime WNP circulation in the second prediction year is further illustrated in Figure 3 for individual models. This figure presents the intermodel spread of late-winter ENSO and springtime WNPM index prediction skills in the second prediction year. Two HadCM3 runs (i.e., triangles in Figure 3), which were initialized 2 months earlier than the other models, are also illustrated. They generally lie within the other five models' ranges. This result suggests that the prediction skills of late-winter ENSO and springtime WNP circulation are not sensitive to the initialization method and month, if the models are initialized in the cold season. The same result is also found in the first prediction year (Figure S5). Here it is worth to note that the MME (i.e., crosses) generally has a higher prediction skill than individual models. More importantly, only MME and CanCM4 show statistically significant ACC skill, which is greater than 0.5, for the spring WNPM index.

Figure 3a clearly shows that the two ACC skills are highly correlated with each other in the second prediction year. The correlation coefficient reaches 0.77 across the seven models. Likewise, MSSS skills are well correlated ($r = 0.67$) at the 90% confidence level (Figure 3b). Although not shown, these values are higher than instantaneous correlations (i.e., MAM NINIO3.4 and MAM WNPM indices). It is further found that the models that have a stronger ENSO-WNPM relationship tend to have a higher prediction skill of spring WNPM index (Figure S6). Thus, the model with a better previous winter's ENSO prediction can reproduce a more reliable spring WNP circulation. This result indicates that the extended prediction skill of the springtime WNP circulation is indeed modulated by the improved ENSO prediction skill in the previous winter.

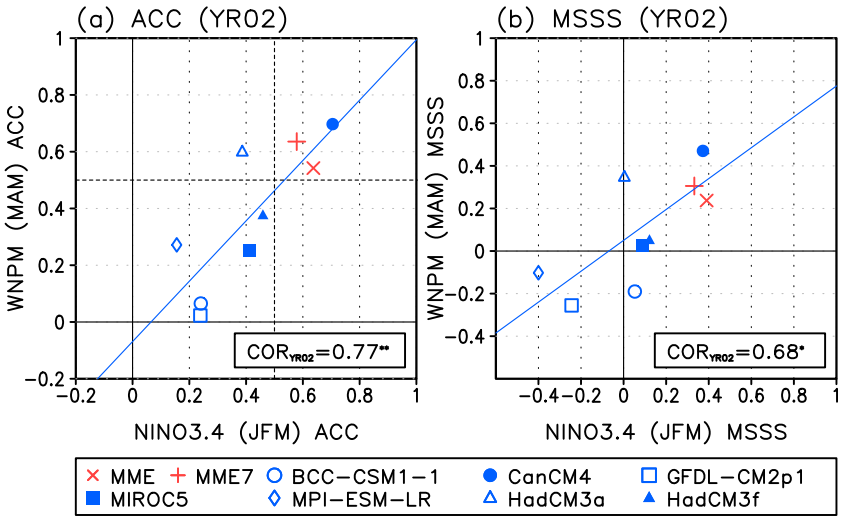

Figure 3. (a) Multimodel spread of ACC of the predicted MAM WNPM index against ACC of the predicted JFM NINO3.4 index in the second prediction year. Multiplication and plus signs indicate the prediction skills from MME and seven-model MME (includes HadCM3a and HadCM3f), respectively. (b) Same as Figure 3a but for the MSSS. Correlation coefficients with two asterisks (an asterisk) indicate that values are statistically significant at the 95% (90%) confidence level.

Figure 4 illustrates the observed and predicted lag correlation map between the MAM WNPM index and the JFM SST. Here SST leads the MAM WNPM index by 2 months. The observed relationship (Figure 4, left) shows that a strong spring WNP circulation is associated with La Niña-like SST anomalies in winter (i.e., anomalous cold SST in the equatorial eastern Pacific and warm SST over the western North Pacific). The MME predictions (Figure 4, middle and right) show similar spatial patterns in both the first and second prediction years. However, correlation coefficients are much higher than observation around the NINO3.4 region (boxed in Figure 4). These results indicate that the dynamical link between the tropical Pacific SST and MAM WNPM index is severely exaggerated in the MME predictions. This stronger-than-observed relationship remains up to the second prediction year, and the exaggerated relationship is also clear in the temporal correlation between JFM NINO3.4 and MAM WNPM indices (i.e., −0.64 for observations but −0.93 and −0.73 for the first and second prediction years). These results indicate that the extended prediction skill of spring WNP circulation more than 1 year in advance likely results from the combined effects of the improved winter ENSO prediction and the exaggerated dynamical coupling between the winter ENSO and spring WNP circulation in the MME prediction.

It is worthwhile noting that significant correlations are found not only over the Pacific but also over the Indian Ocean, particularly in the first prediction year. In contrast to observation (e.g., Figure S3a), the predicted spring WNPM index is highly correlated with the late-winter Indian Ocean SST (see also Figure S3c). The intermodel

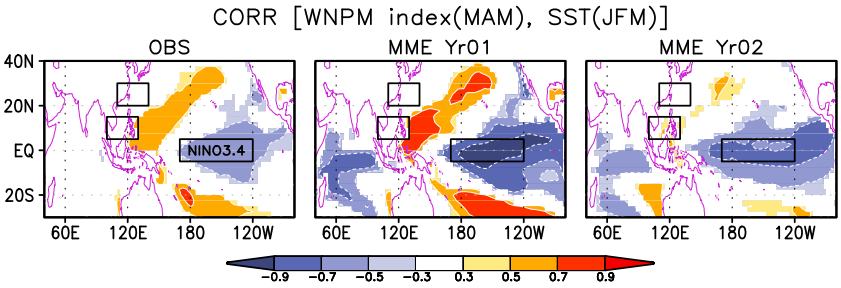

Figure 4. Lagged-correlation coefficient map (shading) between late-winter (JFM) SST field and spring (MAM, 2 month lag) WNPM index from the (left) observation, (middle) first, and (right) second prediction years. The values that are statistically significant at the 95% confidence level are shaded. Black boxes indicate the area where the WNPM and NINO3.4 indices are defined.

spread of the prediction skill of spring WNPM index is also largely explained by the Indian Ocean SST (see blue marks in Figure S5). This may reduce the prediction skill of WNPM index.

4. Conclusions

The MME predictions, based on the CMIP5 decadal hindcast experiments initialized every January from 1981 to 2007, successfully reproduce the springtime atmospheric circulations over the WNP that is quantified by the WNPM index [*Wang et al*., 2001]. Quantitatively, reliable prediction skills are found from the spring to early-summer seasons in the first prediction year (four lead months). Although summer WNPM index can be qualitatively predicted with a maximum lead time of 5 months (i.e., statistically significant ACC that is greater than 0.5), it is not in quantity (i.e., statistically insignificant MSSS). This result holds for individual models regardless of the initialization months (November versus January) and initialization methods (full field versus anomaly initialization).

Somewhat surprisingly, reliable prediction skill of the springtime WNPM index reappears in the second prediction year with a maximum lead time of 14 months. This extended prediction skill is likely caused by the extended prediction skill of winter ENSO up to 12 months in advance and the delayed ENSO impact on the springtime atmospheric circulation in the western North Pacific in MME predictions. However, MME predictions severely exaggerate the later link. The lag correlation, in which ENSO index leads the WNPM index for 2 months, is −0.93 in the first prediction year and this is much higher than the observed correlation (−0.64) indicating that the extended WNPM prediction skill is likely controlled by strong tropical-subtropical teleconnection and highly dependent on the models.

Although further analyses and evaluations are needed, this finding has important implications to the seasonal-to-interannual prediction of the western North Pacific atmospheric circulation. The MME likely filters out climate noises and effectively captures the WNPM circulation. In fact, although all models show significant prediction skills in the first prediction year (Figure S5a), only one model, out of seven models, shows a reliable ACC skill in the second prediction year (Figure 3a). In other words, the exaggerated ENSO-WNPM coupling may result from noise reduction, which could be physically meaningful. If this is the case, the present study would be helpful in improving the interannual prediction of the western North Pacific monsoon circulation.

Acknowledgments

This work was supported by SNU-Yonsei Research Cooperation Program through Seoul National University (SNU) in 2015 and the Basic Science Research Program through the National Research Foundation of Korea (NRF) funded by the Ministry of Education (2013R1A1A1006530). We acknowledge the World Climate Research Programme's Working Group on Coupled Modelling, which is responsible for CMIP, and we thank the climate modeling groups (listed in Table 1 of this paper) for producing and making available their model output. For CMIP, the U.S. Department of Energy's Program for Climate Model Diagnosis and Intercomparison provides coordinating support and led the development of software infrastructure in partnership with the Global Organization for Earth System Science Portals. The ERA-Interim data were obtained from the ECMWF Public Data sets web interface (http://apps.ecmwf.int/datasets/data/interim-full-moda). The GPCP data were provided by the NASA (http://precip.gsfc.nasa.gov/gpcp_v2.2_data.html).

References

Adler, R. F., et al. (2003), The Version-2 Global Precipitation Climatology Project (GPCP) monthly precipitation analysis (1979–present), *J. Hydrometeorol.*, *4*, 1147–1167.

Arora, V. K., J. F. Scinocca, G. J. Boer, J. R. Christian, K. L. Denman, G. M. Flato, V. V. Kharin, W. G. Lee, and W. J. Merryfield (2011), Carbon emission limits required to satisfy future representative concentration pathways of greenhouse gases, *Geophys. Res. Lett.*, *38*, L05805, doi:10.1029/2010GL046270.

Choi, J., S.-W. Son, Y.-G. Ham, J.-Y. Lee, and H.-M. Kim (2016), Seasonal-to-interannual prediction skills of near-surface air temperature in the CMIP5 decadal hindcast experiments, *J. Clim.*, doi:10.1175/JCLI-D-15-0182.1, in press.

Dee, D. P., et al. (2011), The ERA-Interim reanalysis: Configuration and performance of the data assimilation system, *Q. J. R. Meteorol. Soc.*, *137*, 553–597.

Delworth, T. L., et al. (2006), GFDL's CM2 global coupled climate models. Part I: Formulation and simulation characteristics, *J. Clim.*, *19*, 643–674.

Goddard, L., et al. (2013), A verification framework for interannual-to-decadal predictions experiments, *Clim. Dyn.*, *40*, 245–272.

Hu, W., R. Wu, and Y. Liu (2014), Relation of the South China Sea precipitation variability to tropical Indo-Pacific SST anomalies during spring-to-summer transition, *J. Clim.*, *27*, 5451–5467.

Intergovernmental Panel on Climate Change (2013), *Climate Change, 2013: The Physical Science Basis. Contribution of Working Group I to the Fifth Assessment Report of the Intergovernmental Panel on Climate Change*, edited by T. F. Stocker et al., pp. 1535, Cambridge Univ. Press, Cambridge, U. K., and New York.

International CLIVAR Project Office (2011), Data and bias correction for decadal climate prediction. International CLIVAR project Office, CLIVAR Publication Series, 150, 6 pp.

Jin, E. K., et al. (2008), Current status of ENSO prediction skill in coupled ocean-atmosphere models, *Clim. Dyn.*, *31*, 647–664.

Joseph, P. V., J. K. Eishcheid, and R. J. Pyle (1994), Interannual variability of the onset of the Indian summer monsoon and its association with atmospheric features, El Niño and sea surface temperature anomalies, *J. Clim.*, *7*, 81–105.

Lee, J.-Y., et al. (2010), How are seasonal prediction skills related to models' performance on mean state and annual cycle?, *Clim. Dyn.*, *35*, 267–283.

Lee, J.-Y., B. Wang, Q. Ding, K.-J. Ha, J.-B. Ahn, A. Kumar, B. Stern, and O. Alves (2011a), How predictable is the Northern Hemisphere summer upper-tropospheric circulation?, *Clim. Dyn.*, *37*, 1189–1203.

Lee, S.-S., J.-Y. Lee, K.-J. Ha, B. Wang, and J. K. E. Schemm (2011b), Deficiencies and possibilities for long-lead coupled climate prediction of the Western North Pacific-East Asian summer monsoon, *Clim. Dyn.*, *36*, 1173–1188.

Li, C., and M. Yanai (1996), The onset and interannual variability of the Asian summer monsoon in relation to land–sea thermal contrast, *J. Clim.*, *9*, 358–375.

Li, C., R. Lu, and B. Dong (2012), Predictability of the western North Pacific summer climate demonstrated by the coupled models of ENSEMBLES, *Clim. Dyn.*, *39*, 329–346.

Luo, J.-J., S. Masson, S. K. Behera, and T. Yamagata (2008), Extended ENSO predictions using a fully coupled ocean–atmosphere model, *J. Clim.*, *21*, 84–93.

Matei, D., H. Pohlmann, J. Jungclaus, W. Müller, H. Haak, and J. Marotzke (2012), Two tales of initializing decadal climate prediction experiments with the ECHAM5/MPI-OM model, *J. Clim.*, *25*, 8502–8523.

Meehl, G. A., et al. (2014), Decadal climate prediction: An update from the trenches, *Bull. Am. Meteorol. Soc.*, *95*, 243–267, doi:10.1175/BAMS-D-12-00241.1.

Seo, K.-H., J.-H. Son, J.-Y. Lee, and H.-S. Park (2015), Northern east Asian monsoon precipitation revealed by air mass variability and its prediction, *J. Clim.*, *28*, 6221–6233.

Smith, D. M., R. Eade, N. J. Dunstone, D. Fereday, J. M. Murphy, H. Pohlmann, and A. A. Scaife (2010), Skillful multi-year predictions of Atlantic hurricane frequency, *Nat. Geosci.*, *3*, 846–849, doi:10.1038/ngeo1004.

Smith, R. W., et al. (2008), Improvements to NOAA's historical merged land–ocean surface temperature analysis (1880–2006), *J. Clim.*, *21*, 2283–2296.

Stockdale, T. N., D. L. T. Anderson, M. A. Balmaseda, F. Doblas-Reyes, L. Ferranti, K. Mogensen, T. N. Palmer, F. Molteni, and F. Vitart (2011), ECMWF seasonal forecast system 3 and its prediction of sea surface temperature, *Clim. Dyn.*, *37*, 455–471.

Tatebe, H., et al. (2012), Initialization of the climate model MIROC for decadal prediction with hydrographic data assimilation, *J. Meteorol. Soc. Jpn.*, *90A*, 275–294.

Wang, B., R. Wu, and K.-M. Lau (2001), Interannual variability of the Asian summer monsoon: Contrasts between the Indian and the western North Pacific-East Asian monsoons, *J. Clim.*, *15*, 4073–4090.

Wang, B., R. Wu, and T. Li (2003), Atmosphere–warm ocean interaction and its impacts on Asian–Australian monsoon variation, *J. Clim.*, *16*, 1195–1211.

Wang, B., J.-Y. Lee, I.-S. Kang, J. Shukla, J.-S. Kug, A. Kumar, J. Schemm, J.-J. Luo, T. Yamagata, and C.-K. Park (2008), How accurately do coupled climate models predict the Asian–Australian monsoon interannual variability?, *Clim. Dyn.*, *30*, 605–619.

Wang, B., B. Xiang, and J.-Y. Lee (2013), Subtropical high predictability establishes a promising way for monsoon and tropical storm predictions, *Proc. Natl. Acad. Sci. U.S.A.*, *110*, 2718–2722.

Wu, R., and W. Hu (2015), Air-sea relationship associated with precipitation anomaly changes and mean precipitation anomaly over the South China Sea and the Arabian Sea during the spring to summer transition, *J. Clim.*, *28*, 7161–7181.

Wu, T., et al. (2014), An overview of BCC climate system model development and application for climate change studies, *J. Meteorol. Res.*, *28*, 34–56.

Xie, S.-P., et al. (2009), Indian ocean capacitor effect on Indo–western Pacific climate during the summer following El Nino, *J. Clim.*, *22*, 730–747.